DE GRUYTER OPEN

Acta Geophysica
vol. 64, no. 5, Oct. 2016, pp. 1225-1256
DOI: 10.1515/acgeo-2016-0048

Hybrid-Empirical Ground Motion Estimations for Georgia

Nino TSERETELI[1], Aysegul ASKAN[2], and Hossein HAMZEHLOO[3]

[1]Institute of Geophysics of Tbilisi State University, Tbilisi, Georgia;
e-mails: nino66_ts@yahoo.com; nino_tsereteli@tsu.ge

[2]Middle East Technical University, Ankara, Turkey; e-mail: aaskan@metu.edu.tr

[3]International Institute of Earthquake Engineering Seismology, Tehran, Iran;
e-mail: hhamzehloo@yahoo.com

A b s t r a c t

Ground motion prediction equations are essential for several purposes ranging from seismic design and analysis to probabilistic seismic hazard assessment. In seismically active regions without sufficiently strong ground motion data to build empirical models, hybrid models become vital. Georgia does not have sufficiently strong ground motion data to build empirical models. In this study, we have applied the host-to-target method in two regions in Georgia with different source mechanisms. According to the tectonic regime of the target areas, two different regions are chosen as host regions. One of them is in Turkey with the dominant strike-slip source mechanism, while the other is in Iran with the prevalence of reverse-mechanism events. We performed stochastic finite-fault simulations in both host and target areas and employed the hybrid-empirical method as introduced in Campbell (2003). An initial set of hybrid empirical ground motion estimates is obtained for PGA and SA at selected periods for Georgia.

Key words: earthquakes, hybrid-empirical ground motion model, seismotectonics, strong-motion database, ground motion simulations.

1. INTRODUCTION

Given earthquake magnitude, source-to-site distance and soil conditions, predictive models yield anticipated ground motion levels expressed in terms of peak ground parameters or the corresponding spectral quantities. In addition to being used widely for earthquake engineering purposes, predicted ground motion levels are key elements of quantitative estimation of probabilistic seismic hazard (PSHA) and they govern most of the uncertainties in computed hazard levels. In recent studies, it is discussed that the vital component that influence the calculated hazard is ground motion prediction equations (GMPE) (*e.g.*, Cotton *et al.* 2006), and that in particular the aleatory and epistemic uncertainties of the GMPEs affect the results considerably. Among these two, epistemic uncertainty is handled in the analyses via a logic-tree approach. Concerning aleatory uncertainty, it is difficult to reduce it even for regions with dense seismic arrays and large databases of strong-motion records (Douglas 2003). In recent studies, it is observed that the effect of various parameters such as site classes Vs30, fault type on aleatory uncertainty is very low (*e.g.*, Boore 2004, Bommer *et al.* 2003). The large aleatory variability is accounted for using simple models in GMPEs for defining complex phenomena (Bommer and Abrahamson 2007). Thus, reduction of aleatory variability in predictive models used within PSHA framework still remains a fundamental problem.

Issues concerning uncertainty in seismic hazard assessment become more predominant for regions with sparse seismic networks and/or poor strong motion data. Both the epistemic uncertainty and aleatory variability is increased in such cases. A practical application for regions of sparse data is the hybrid empirical method (HEM) developed by Campbell (2003). The hybrid empirical method uses the ratio of stochastic ground motion estimates to adjust empirical ground-motion relations developed for host region (with abundant data) to use in another target region (with sparse data). GMPEs established for host region are transferred to the target region using regional adjustment factors derived from stochastic simulations performed in both host and target regions. Such applications are performed for eastern North America (Pezeshk *et al.* 2011), southern Norway and southern Spain (Douglas *et al.* 2005), and eastern Mediterranean region (Cagnan 2013).

In this study, we developed an initial set of hybrid empirical ground motion estimates in terms of PGA and SA at selected periods for Georgia. We picked two regions of well known seismicity and past data in Georgia as the target regions: Javakheti and Racha regions. Before going into details of the host to target methodology and the study regions, we present background information on seismotectonics of Georgia, current strong motion database and previous empirical ground motion models.

2. SEISMOTECTONICS OF GEORGIA

The Republic of Georgia is located between the Russian Federation in the north, Turkey and Armenia in the south. The main morphological units of Georgia are the mountain ranges of the Greater and Lesser Caucasus separated by the Black Sea − Rioni and Kura (Mtkvari) − South Caspian intermountain troughs. Recent geodynamics of Georgia and adjacent territories of the Black Sea − Caspian Sea region are determined by the still-converging Eurasian and Africa–Arabian plates. Related tectonic activities cause moderate seismicity in the region. According to geodetic data, the rate of convergence is 20-30 mm/y, around 2/3 of which are likely to be taken up south of the Lesser Caucasian (Sevan–Akera) ophiolitic suture, mainly in south Armenia, Nakhchivan, northwest Iran, and Eastern Turkey. The rest of the South-North directed relative plate motion has been accommodated in the South Caucasus mostly by crustal shortening (DeMets *et al.* 1990, Jackson and Ambraseys 1997, Allen *et al.* 2004, Reilinger *et al.* 2006).

Three principal directions of active faults compatible with the dominant near N-S compressional stress produced by northward displacement of the Arabian plate can be distinguished in the region (Fig. 1): one longitudinal (WNW-ESE or W-E) and two transversal (NE-SW and NW-SE). The first set is called the Caucasian strike and it is represented by compressional structures: reverse, thrusts, and napes. The second set consists of transversal faults which are also mainly compressional structures having somewhat considerable strike-slip components. The final set of faults has tensional nature

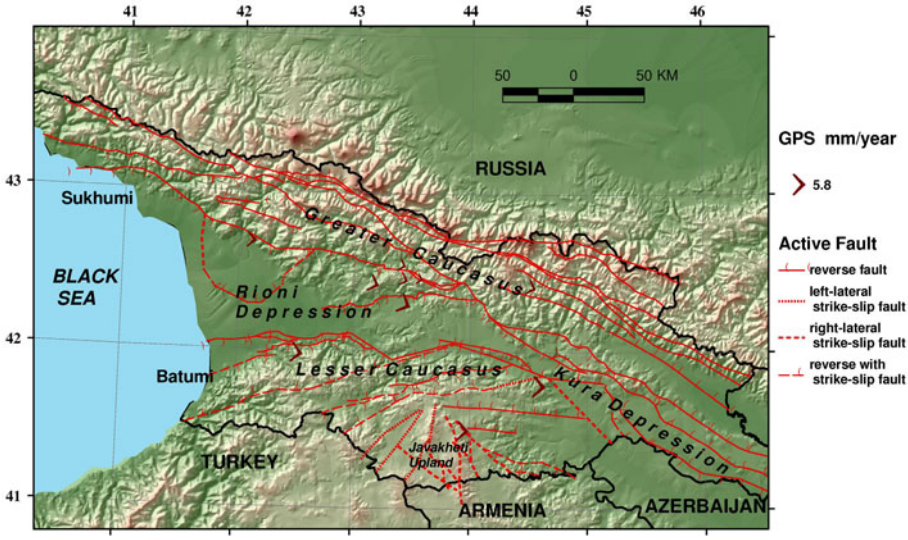

Fig. 1. Map of active structures in Georgia.

of sub-meridian faults, as evidenced by intensive Neogene–Quaternary volcanism related to these faults in some areas of Southern Georgia (Javakheti Highland) and the Greater Caucasian range. Southern parts of Georgia include mainly NE-SW left-lateral strike-slip faults similar to the structures in Northeastern Turkey and Armenia.

Over the past, historical period of time in Georgia, the observed seismicity is characterized as moderate. All historical and instrumentally observed strong and moderate earthquake sources ($4.5 < Ms < 7$) were located along the active fault systems of the Greater and Lesser Caucasus and intermountain depressions. The earthquake distributions in terms of fault plane solutions for moderate and strong earthquakes show only three stress regimes as SS (strike slip), T (thrust fault), and TS (thrust strike), while a similar observation for the smaller earthquakes show all types of stress regimes. Therefore, the moderate and strong earthquakes reflect the regional tectonics. By this classification, southern slopes of the Greater Caucasus are characterized by mostly thrust and thrust strike mechanisms, while the Javakheti Upland is characterized by mostly strike slip faults. Finally, the Kura depression is defined with thrust-right lateral strike slips (Varazanashvili *et al.* 2012).

In a recent study, Varazanashvili *et al.* (2011) showed that the distribution of earthquakes by depth yields three main depth ranges: Δh_1 = 3-8 km, Δh_2 = 8-13 km, and Δh_2 = 13-18 km. They also showed that the first depth range is associated with relevantly weak earthquakes ($M < 5$) while the second and third ones – with strong earthquakes ($M \geq 5$).

Among the described structures, in this study, two different tectonic regime units are chosen in Georgia for the application of hybrid-empirical method: active faults of Great Caucasus (Racha area) with thrust faulting regime and Southern Georgia (Javakheti Upland) with strike-slip faulting regime.

3. GEORGIAN STRONG-MOTION DATABASE AND DATA PROCESSING

Digital accelerograph network in the Caucasus area was previously operated by three agencies: the National Survey of Seismic Protection of the Republic of Armenia, the Georgian Academy of Sciences, and the Swiss Seismological Service granted by the Swiss Disaster Relief. This initial network, which has become operational in 1990, was gradually extended after the 29 April 1991 Racha earthquake (Ms = 6.9, Georgia). At the time of the earthquake, the network consisted of 12 digital free-field stations, 16 analog strong-motion stations, 6 digital strong-motion instruments for aftershock studies, and 2 structural monitoring related arrays (Smit *et al.* 2000). In 2006 digital strong-motion network in Georgia stopped working and there is no accelerograph

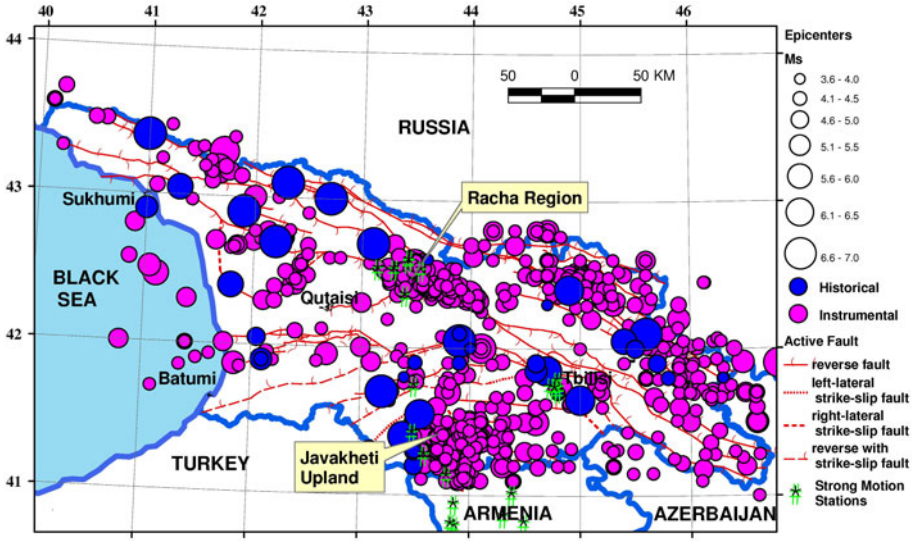

Fig. 2. Distribution of the stations within the Georgian strong motion network during the period 1990-2006.

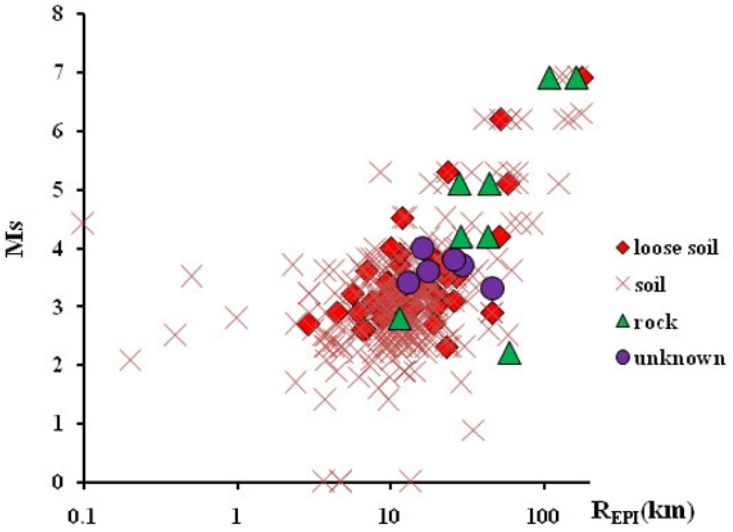

Fig. 3. Distribution of Georgian SM data in terms of magnitude *versus* epicentral distance (R_{EPI}) with respect to different soil conditions.

network as of today. The existing strong ground motion dataset includes 558 acceleration time histories from 314 earthquakes occurred in the South Caucasus (SC). The events have magnitudes that range between 0.5 and 7 while the epicentral distances of the records vary within 1-178 km. We note that

376 of the records are from earthquakes that occurred in Georgia and remaining are from those in Armenia. Figure 2 shows the stations of the strong motion network in Georgia during the 1990-2006 period and distribution of the earthquakes with recorded ground motion data.

Figure 3 displays the distance distribution of the magnitudes of the past events with respect to different soil conditions of the recording stations. It is observed that most of the near-fault data are from small to moderate earthquakes with magnitude $Ms \leq 4.5$. Most of these data are recorded only at one station. The number of records for earthquakes with $Ms \geq 2.9$ ($Mw \geq 4$) that are recorded at more than one station is 88 for Georgia. As mentioned before, the data is mainly from the Racha zone and Javakheti Upland shown in Fig. 2. In addition, it should be noted that in the earthquake catalog of Georgia, magnitudes were categorized with respect to surface wave magnitude (*Ms*). Since 1960, the energy class (*K*) of earthquakes was used in cases when the direct determination of the magnitude *Ms* was impossible. *Ms* in such cases was estimated mainly by the Rautian equation (Rautian 1960):

$$Ms = 0.55\,K - 2.2\ . \tag{1}$$

Since 2004, as a consequence of the reorganization of the seismic network in Georgia, only local magnitude *Ml* was estimated for earthquakes and rarely the magnitude scales *md* and *mb*. Thus, the catalog was complied in terms of *Mw*. In this case, conversion to the magnitude *Ms* was carried out by the correlation given in Zare *et al.* (2014):

$$Mw = 0.66\,Ms + 2.11 \quad \text{if} \quad 2.8 \leq Ms \leq 6.1\ , \tag{2}$$

$$Mw = 0.93\,Ms + 0.45 \quad \text{if} \quad 6.2 \leq Ms \leq 8\ , \tag{3}$$

$$Mw = 0.87\,mb + 0.83 \quad \text{if} \quad 3.5 \leq mb \leq 6.0\ , \tag{4}$$

$$Mw = 1.01\,Ml - 0.05 \quad \text{if} \quad 4.0 \leq Ml \leq 8.3\ . \tag{5}$$

In this study, unprocessed ground motion records are filtered according to the procedures described in Akkar and Bommer (2006) and Akkar *et al.* (2011). Finally, the database for Georgian strong motion records is reorganized as follows: event parameters such as time of occurrence, epicentre coordinates, magnitude (and fault plane solution whenever available), station location, and site classification by geological data; processed data with all steps followed in data processing.

Figure 4 presents the distribution of processed PGA with respect to distance and soil conditions. Site classification was performed from a geological map of the region (1:50 000). As of now, there are no Vs30 estimations or borehole data for Georgian SM stations.

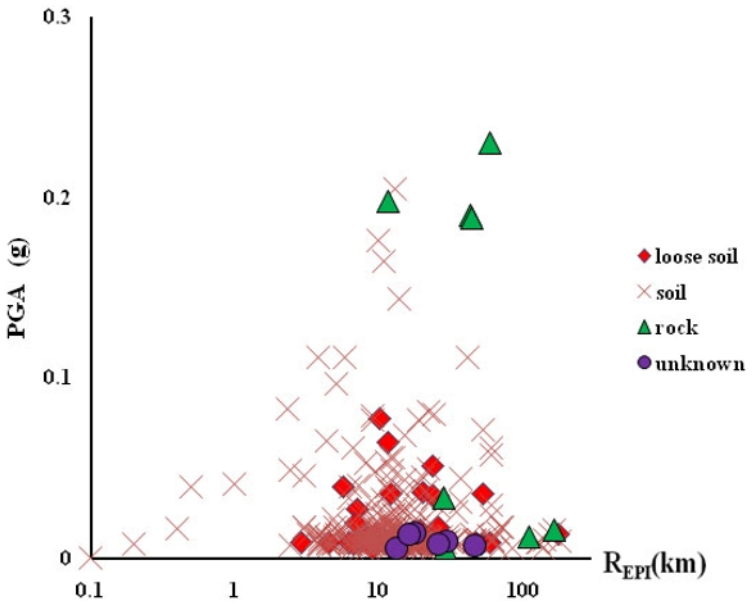

Fig. 4. Distribution of PGA *versus* epicentral distance (R_{EPI}) with respect to different soil conditions (Georgian SM database).

4. PREVIOUS EMPIRICAL GROUND MOTION MODELS IN GEORGIA

Despite the lack of systematic strong motion data collection in Georgia, there are some predictive models proposed for this region. Smit *et al.* (2000) proposed a ground motion prediction model in the form of:

$$\log Y = a + b \cdot M + c \cdot \log R + d \cdot R + p \cdot \varepsilon \ , \quad R = \sqrt{D^2 + h^2} \ , \tag{6}$$

where Y is the absolute acceleration response (maximum horizontal), SA with 5% damping [cm/s^2], M is the surface-wave magnitude, and D is the hypocentral-distance [km]. The value of p is 0 for 50-percentile values and 1 for 84-percentile. The equation is derived based on a dataset that consists of 407 acceleration time histories within a magnitude (*Ms*) range of (1.5-07.1) recorded within distances between 1 and 117 km for the Caucasus, Turkey (northeast part), and Iran, also additional 200 acceleration time histories for Kirgisia, southern Kuril Islands (Russia), Sachalin, Russia, for *Ms* range 2-6.8 between 4-57 km distances.

The resulting equation for larger horizontal values of peak horizontal acceleration [cm/s^2] is:

$$\log pha = 0.72 + 0.44 \cdot M - \log R - 0.00231 \cdot R + 0.28 \cdot p \ , \quad R = \sqrt{D^2 + 4.5^2} \ . \tag{7}$$

Coefficients of the attenuation relationship for absolute acceleration response (larger horizontal) SA for 5% critical damping are presented in Table 1.

Table 1

Coefficients of the attenuation relationship
for absolute acceleration response (larger horizontal) SA for 5% critical damping

Frequency [Hz]	Larger spectral horizontal ground motion on alluvium					
	a	*b*	*c*	*d*	*h*	ε
1.0	–1.733	0.804	–1.0	–0.00237	1.0	0.38
1.5	–1.673	0.846	–1.0	–0.00301	0.0	0.40
2.0	–1.150	0.778	–1.0	–0.00273	6.0	0.40
2.5	–0.890	0.768	–1.0	–0.00399	8.5	0.39
3.0	–0.739	0.767	–1.0	–0.00492	6.5	0.39
4.0	0.052	0.632	–1.0	–0.00437	9.0	0.34
5.0	0.390	0.570	–1.0	–0.00341	6.5	0.31
6.0	0.841	0.472	–1.0	–0.00167	5.5	0.30
7.0	1.111	0.419	–1.0	–0.00152	4.5	0.27
8.0	1.433	0.355	–1.0	–0.00139	4.5	0.28
9.0	1.706	0.303	–1.0	–0.00117	5.5	0.28
10.0	1.955	0.254	–1.0	–0.00095	6.0	0.28
11.0	1.840	0.279	–1.0	–0.00158	5.0	0.28
12.0	1.834	0.275	–1.0	–0.00145	4.5	0.29
13.0	1.843	0.266	–1.0	–0.00109	4.0	0.29
14.0	1.690	0.298	–1.0	–0.00154	4.0	0.29
15.0	1.587	0.318	–1.0	–0.00186	4.0	0.30
16.0	1.591	0.309	–1.0	–0.00149	2.0	0.30
17.0	1.533	0.319	–1.0	–0.00151	0.0	0.30
18.0	1.454	0.332	–1.0	–0.00149	0.0	0.29
19.0	1.341	0.351	–1.0	–0.00159	0.0	0.29
20.0	1.301	0.358	–1.0	–0.00185	0.0	0.29

Another predictive model was developed by Slejko *et al*. (2008) within the frame of the project "Seismic Hazard Assessment for the Tbilisi Test Area" (SETA). The SETA ground motion prediction equation was calibrated on data from the European strong motion data bank (Ambraseys *et al.* 2000, 2004) that belong to earthquakes that occurred in Caucasus (36°-46° N, 38°-52° E). The attenuation model used has the following functional form:

$$\log_{10} \mathrm{PGA} = a + \left(b + cM_S\right) M_S + \left(d + eM_S\right) \log_{10} r \quad \text{with} \quad r^2 = \Delta^2 + h^2 \ , \quad (8)$$

where PGA is expressed in g, Δ is the epicentral distance in km, while a, b, c, d, e, and h are parameters estimated through regressions on the available dataset. The resulting relation for PGA is as follows:

$$\log_{10}\mathrm{PGA} = -2.14+\left(0.98-0.06M_S\right)M_S+\left(-1.88+0.0009M_S\right)\log_{10}r \quad \text{with} \quad h=13.4. \tag{9}$$

This relation is considered valid for an epicentral distance shorter than 100 km.

Considering the very few previous ground motion models proposed for the region in addition to the existing insufficient strong motion dataset, the need for hybrid-empirical models has become apparent for Georgia and surrounding areas.

5. HYBRID EMPIRICAL GROUND MOTION ESTIMATES FOR GEORGIA

In this study, we made hybrid empirical ground motion estimations for two different tectonic regions in Georgia using the method proposed by Campbell (2003). The fundamental objective of the methodology is to form ground motion relations for a target region with sparse strong motion networks or fewer strong motion data from a host region with existing ground motion models and abundant data through the use of adjustment factors. These ground motion adjustment factors are calculated based on stochastic ground motion simulations in both target and host regions. For space limitations, the details of the algorithm and the entire mathematical framework will not be repeated herein but the method will be described shortly next.

5.1 Method

The basic steps of the hybrid empirical method are as follows (Campbell 2003): (i) selection of the host and target regions, (ii) calculation of empirical ground-motion estimates for the host region, (iii) calculation of seismological-based adjustment factors between the host and target regions, (iv) calculation of hybrid empirical ground-motion estimates for the target region, and (v) development of ground-motion relations for the target region. The detailed mathematical framework with the original notation containing multiple values of each model parameter could be found in Campbell (2003).

Herein, for simplicity of the notation, we present the median hybrid empirical ground-motion estimate in the target region in general terms as follows:

$$\ln\left(\mathrm{HE}-\mathrm{GMP}\right)_{\mathrm{TARGET}} = \sum_{i=1}^{n} w_i \left(\ln C + \ln E - \mathrm{GMP}(i)_{\mathrm{HOST}}\right) , \tag{10}$$

where $\ln (\mathrm{HE-GMP})_{\mathrm{TARGET}}$ is the natural logarithm of the hybrid-empirical estimate of the selected ground motion parameter (GMP) such as PGA or SA at a certain period in the target region; $E-\mathrm{GMP}(i)_{\mathrm{HOST}}$ is the natural logarithm of the empirical estimate of the corresponding GMP in the host region obtained from the i-th GMPE; C is the median value of the seismological-based adjustment factor between host and target regions; w_i is a set of weights whose sum is equal to unity; and n is the total number of empirical ground motion models (GMPEs) used in the calculations. The seismological-based adjustment factors between host and target regions (C) are simply the ratios of the modeled (simulated) ground-motion estimate in the target region to the modeled ground-motion estimate in the host region for a given set of magnitudes, distances, and selected seismological parameters.

In this study, we note that we perform and present the results obtained at the fourth step of the original algorithm of Campbell (2003) where the hybrid-empirical ground motion estimates are obtained for Georgia and compared with the observations, as presented in Section 5.4.

5.2 Study regions

In this study, we picked two regions of well known seismicity in Georgia as the target regions: Javakheti and Racha (Figs. 5 and 6). To be consistent with the tectonic regime in the target regions, two areas are chosen as the corresponding host regions: one of them is the North Anatolian Fault zone in Turkey with mostly strike-slip stress regime and the other is Tabas in Iran with mostly reverse mechanism.

The Javakheti polygon roughly coincides with the volcanic highland of the same name located in South Georgia, at the boundary with Turkey and Armenia. This is the most seismically active region for Georgia. This highland represents a young tectonic unit formed during Neogene–Quaternary era. The entire territory of the highland is covered by thick volcanic rocks (basalts, andesites, dacites, and rhyolites) that erupted in subaerial environments during the last 9 million years. The strongest earthquake occurred there in 1986, with $Ms = 5.6$ ($Mw = 5.8$). Distribution of epicenters in Javakheti shows their isometric clustering (Fig. 5). Focal mechanisms reveal the complex nature of seismically active structures whose predominant form is strike slip.

The second region that was considered is Racha region which is one of the most active regions in Georgia. The 29 April 1991 Racha earthquake ($Ms \sim 6.9$, $Mw = 6.9$), the largest instrumentally-recorded event in Georgia, is also one of the strongest recent earthquakes in the Caucasus. The aftershocks form a zone around 90 km long and 20-30 km wide striking W-E, following the Racha–Lechkhumi suture zone at the southern boundary of the

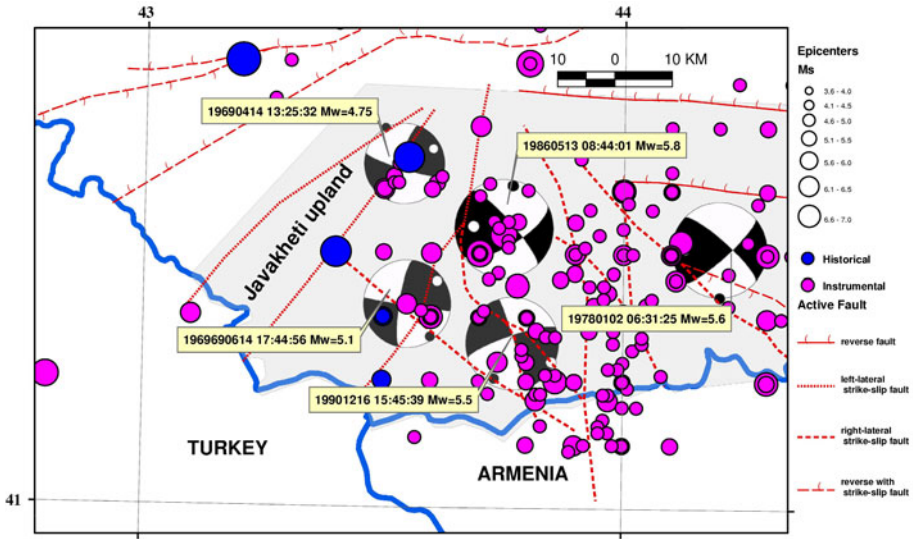

Fig. 5. Seismicity and source mechanisms in Javakheti region (Georgia).

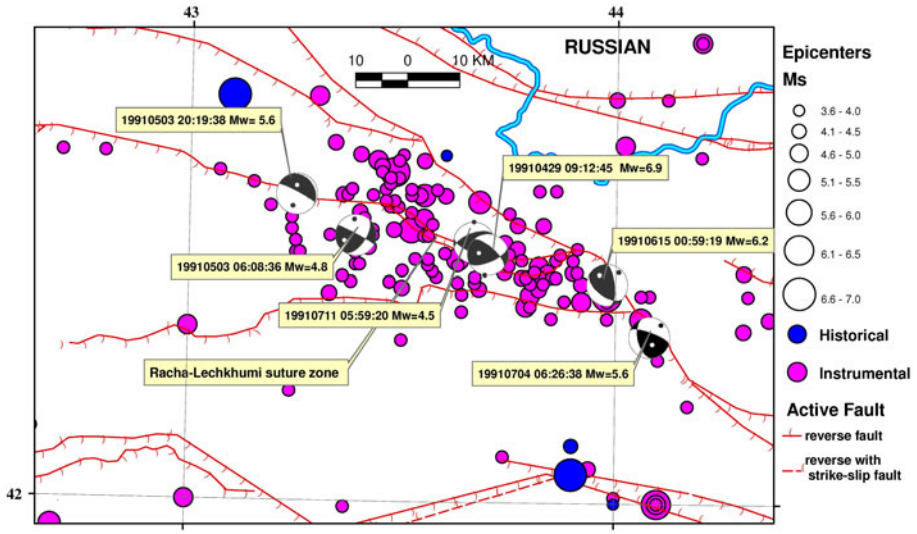

Fig. 6. Seismicity and source mechanisms in Racha region (Georgia).

Greater Caucasian southern slope. Teleseismic data on Racha earthquake aftershocks from 15 May to 15 June 1991 reveal two main clouds of shocks, trending WNW 290° and NW 310°, respectively, converging south-eastward and merging together near Tskhinvali. Both the geological evidence and focal mechanism solutions indicate that Racha fault system is dominated by compressional structures of reverse faults (Fig. 6).

5.3 Verification of simulation parameters for Georgia

In this study, as the host regions, we use the North Anatolian Fault zone (Turkey) which generates mostly strike-slip events (host for Javakheti region) and the Tabas region in Iran producing earthquakes with reverse mechanisms (host for Racha region). These host regions are selected since they both have well-established empirical ground motion relations. The second step is naturally achieved as both Turkey and Iran have several well-studied empirical ground motion prediction equations (*e.g.*, Akkar *et al.* 2010, Amiri *et al.* 2007). The third step of the algorithm requires ground motion simulations: Campbell (2003) used point-source stochastic models whereas in this study we employed finite-fault stochastic simulations based on the algorithm outlined in Motazedian and Atkinson (2005). In this step, an important point is the accuracy of input simulation parameters: for Iran and Turkey, well-established parameters existed already (*e.g.*, Ugurhan and Askan 2010, Askan *et al.* 2013, Shoja-Taheri and Ghofrani 2007, Zafarani *et al.* 2009). However, for Georgia no extensive simulations had been performed previously other than the study of Sokolov (1997) where small to moderate ($Ms \leq 6.2$) earthquakes obtained in the epicentral area of the 29 April 1991 Racha earthquake, ($Ms = 6.9$) were simulated. Since there are no established simulation parameters for the region, we initially verified the existing input parameters through simulations of selected major events in both Javakheti and Racha regions.

5.3.1 Simulation of the 16 December 1990 Javakheti earthquake (Mw = 5.5)

In this study, we initially simulated the 16 December 1990 Javakheti earthquake ($Mw = 5.5$). The source parameters of the event ($Ms = 5.1$, $Mw = 5.5$, lat. = 41.35, long. = 43.78, depth = 9 km, strike = 342.68, dip = 85.04, and rake = 164.5) are taken from the Georgian strong motion databases. The relationship between magnitude and earthquake source size was adopted from Riznichenko (1992). This relationship was derived from empirical data for Caucasian and central Asian earthquake and it worked effectively in the simulations. Stress drop of this event is estimated to be 70 bars through the empirical formula presented in Riznichenko (1992). We use the regional intrinsic attenuation (Q) model in the form $Q = 37f^{1.089}$ as estimated by Shengelia *et al.* (2011). As far as the kappa factor is concerned, for the rock and soil stations we used kappa values of 0.035 and 0.052, respectively. We used a geometrical spreading function of the form $1/R$. The event is simulated at the stations whose information is presented in Table 2. The observed *versus* simulated acceleration time histories and the corresponding Fourier amplitude spectra at the BVR, TRS, and SAK stations are shown in Figs. 7-12. Figure 7 shows that at BVR (Bavra) station, the simulated time history

Table 2

Information on Strong Motion Stations
which recorded the16 December 1990 Javakheti earthquake

Station code and name	Latitude (N)	Longitude (E)	Site class	Epicentral distance [km]
BVR Bavra	41.120	43.809	Rock	142
TRS Toros	40.928	43.873	Soil	163
SAK Akhalkalaki	41.410	43.493	Rock	24
BGD Gogdanovka	41.265	43.600	Soil	7
BKR Bakuriani	41.734	43.502	Rock	47

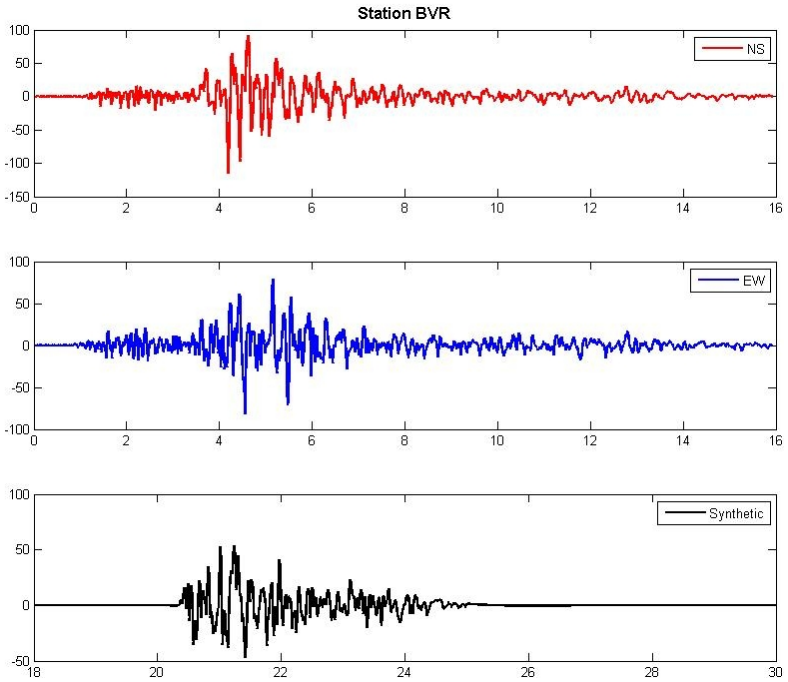

Fig. 7. Simulation results for Javakheti earthquake (16 December 1990) on BVR station. The observed *versus* simulated acceleration time histories.

matches the observed accelerograms (particularly the EW component) in terms of both duration and amplitude content. Figure 8 shows that in the frequency domain, despite the close fit at the lower and higher frequencies, there is slight discrepancy between the observed and simulated spectra around 1 Hz where there is possibly an amplification peak that could not be

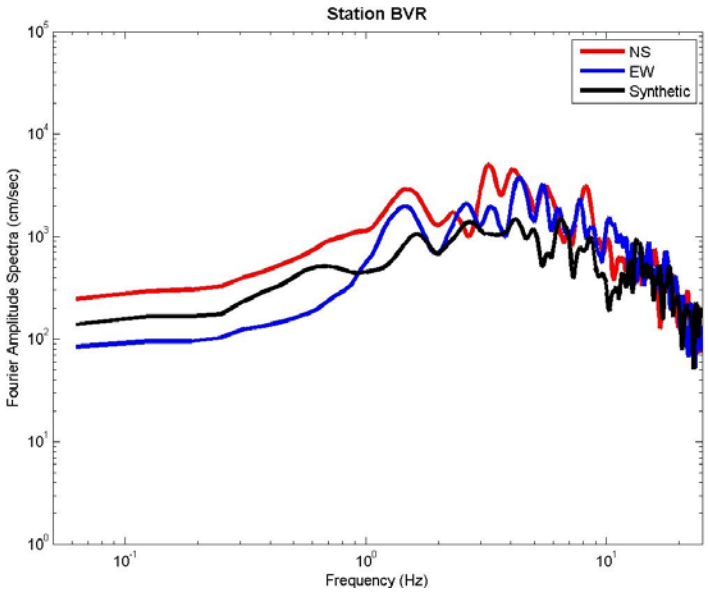

Fig. 8. Simulation results for Javakheti earthquake (16 December 1990) on BVR station. Fourier amplitude spectra.

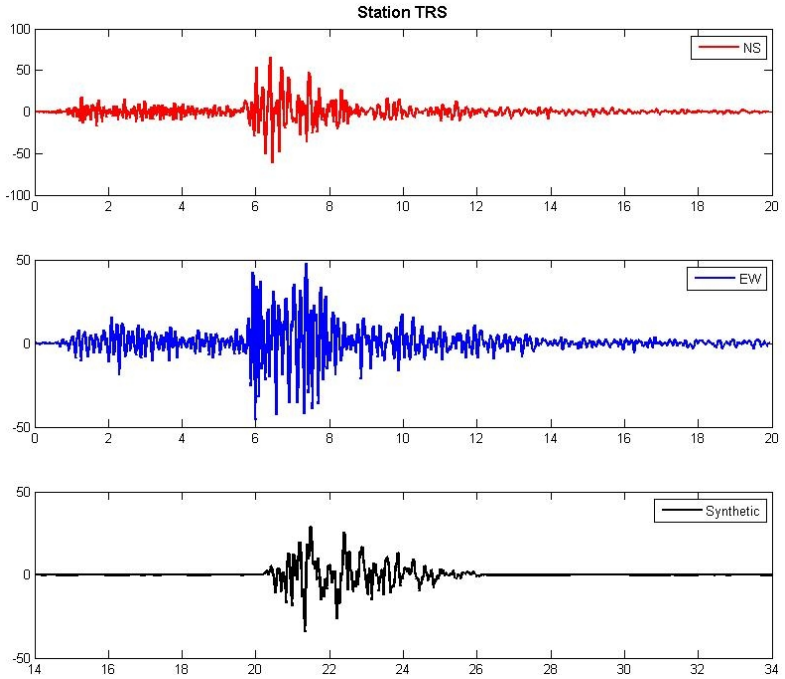

Fig. 9. Simulation results for Javakheti earthquake (16 December 1990) at TRS station. The observed *versus* simulated acceleration time histories.

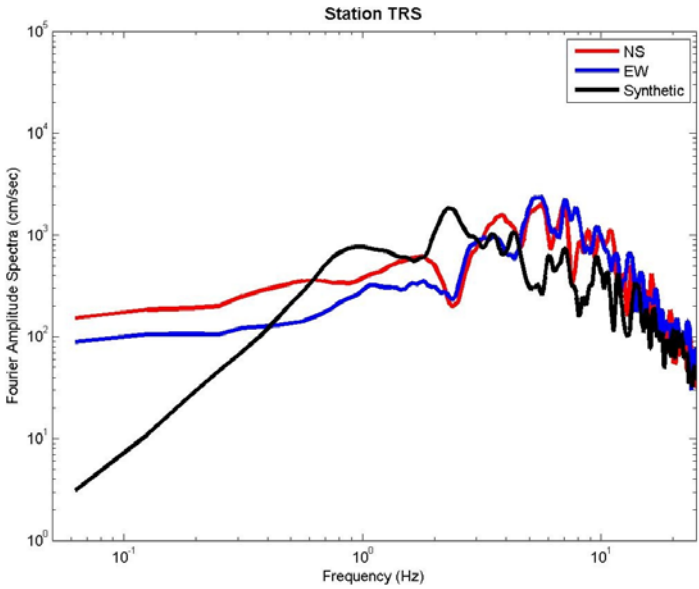

Fig. 10. Simulation results for Javakheti earthquake (16 December 1990) at TRS station. Fourier amplitude spectra.

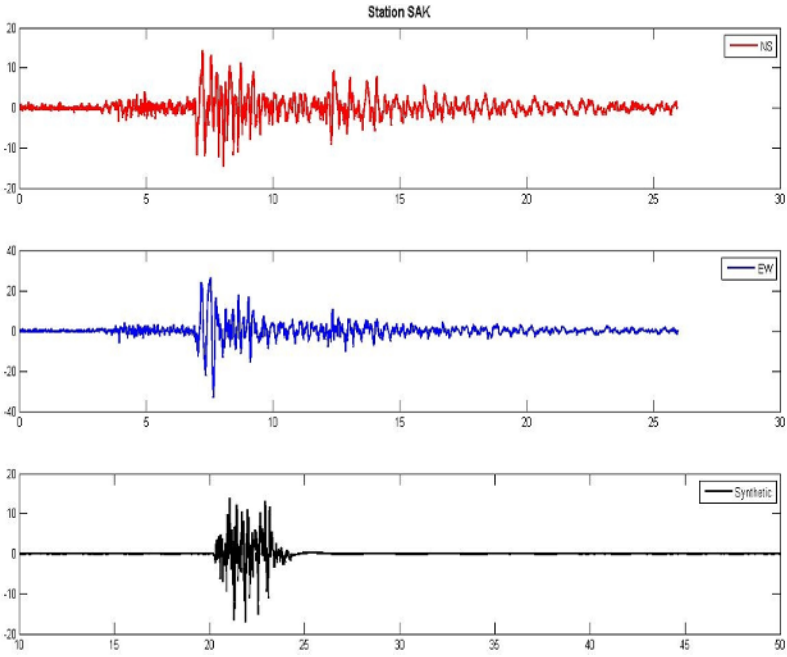

Fig. 11. Simulation results for Javakheti earthquake (16 December 1990) at SAK station. The observed *versus* simulated acceleration time histories.

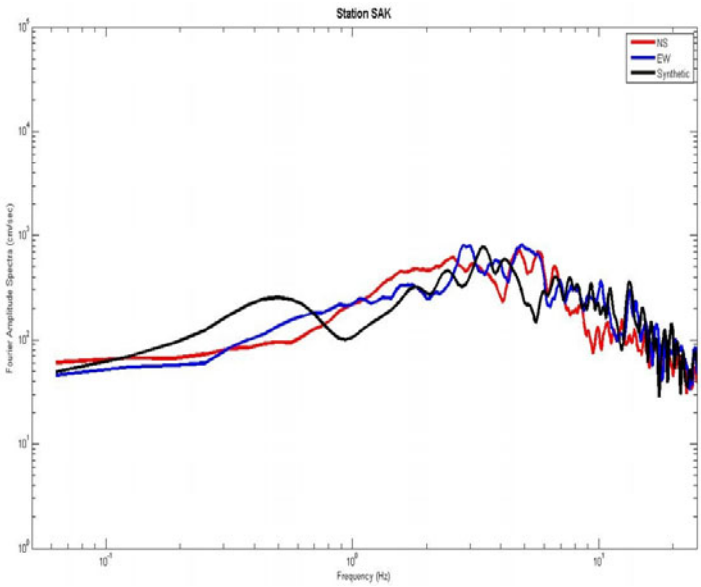

Fig. 12. Simulation results for Javakheti earthquake (16 December 1990) at SAK station. Fourier amplitude spectra.

simulated. Figures 9 and 10 demonstrate that the fit for station TRS (Toros) is close in terms of amplitudes and duration but the match in terms of frequency content is not as effective. The synthetic record underestimates the observations, in particular for intermediate frequencies of 2-10 Hz. Since the TRS station is located on soil, this discrepancy could be attributed to the local site response that was not effectively simulated. Figure 11 shows that the simulated data at SAK (Akhalkalaki) station matches the observed NS component closely in terms of PGA values and duration of the *S*-waves but the surface waves observed in the records could not be simulated in the stochastic method used herein. In Fig. 12, we observe that there is a close match at frequencies higher than 1 Hz, but at frequencies less than 1 Hz, there is a clear mismatch. Station SAK is located at 7 km from the epicenter of the event and the low frequency misfit is most probably due to source effects that could not be simulated in the stochastic finite-fault method. In some cases, near-field records require more complex source models than the ones stochastic method employs (*e.g.*, Ugurhan and Askan 2010).

To quantify the goodness of fit in the simulations, we define a misfit function in the frequency domain for each station as follows:

$$E(f) = \log\left(\frac{\mathrm{FAS}_i(f)_{\mathrm{observed}}}{\mathrm{FAS}_i(f)_{\mathrm{synthetic}}}\right), \tag{11}$$

where $FAS_i(f)_{observed}$ is the observed Fourier amplitude spectrum, $FAS_i(f)_{synthetic}$ is the synthetic Fourier amplitude spectrum, f is the frequency of interest. Figures 13-15 display the corresponding misfit functions for the 16 December 1990 Javakheti earthquake simulation at BVR, TRS, and SAK stations, respectively. The misfits indicate that there is no bias towards over-estimation or underestimation of the observed spectra. Finally, overall we conclude that the simulation results do not yield perfect matches with the records at all stations but the validations are sufficient to employ an initial application of the hybrid-empirical method for Georgia.

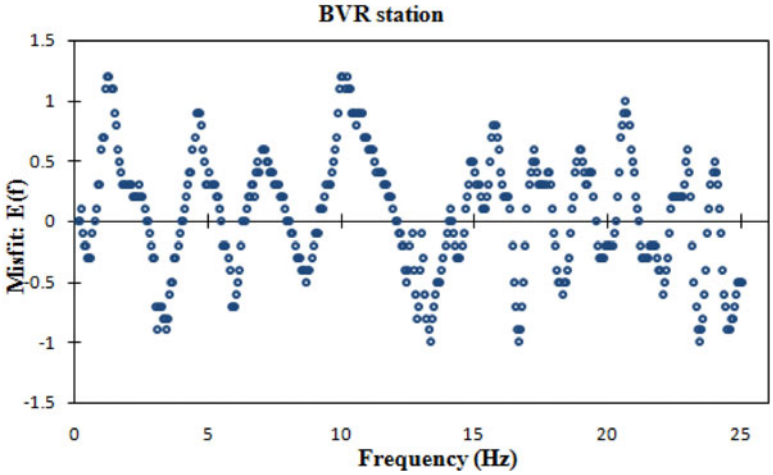

Fig. 13. Misfit function for the 16 December 1990 Javakheti earthquake simulation at BVR station.

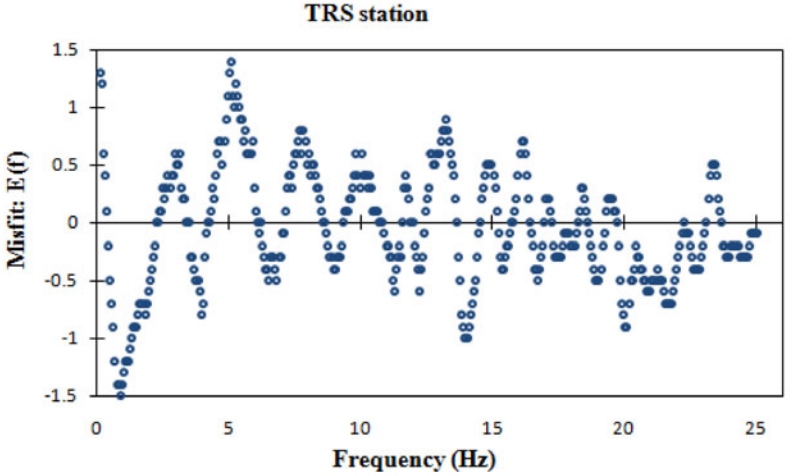

Fig. 14. Misfit function for the 16 December 1990 Javakheti earthquake simulation at TRS station.

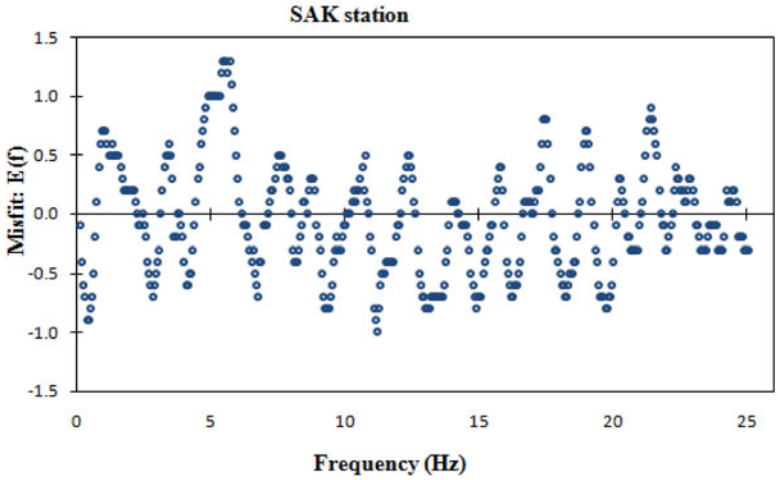

Fig. 15. Misfit function for the 16 December 1990 Javakheti earthquake simulation at SAK station.

5.3.2 Simulation of the 29 April 1991 Racha earthquake (Ms = 6.9)

Similarly, we performed stochastic finite fault simulation of the 29 April 1991 Racha earthquake. The following source parameters are used: Mw = 6.9, lat. = 42.424, long. = 43.664, depth = 8 km, strike = 99.0, dip = 51, and rake = 128. We employed an attenuation model in the form $Q = 77f^{0.937}$. Kappa values are defined as in the Javakheti simulations. We used a geometrical spreading function of the form $1/R$. Information on the strong motion station used in simulations is given in Table 3. We also simulated the 3 May 1991 Racha earthquake. Figures 16-19 display the results of these simulations at IRI and ONB stations located in the near-field area. Figures 16 and 17 show that at IRI station the lower frequencies are not represented well, most probably due to source effects, yet for higher frequencies the match between the observed and synthetic FAS is close. Figures 18 and 19 show that at ONB station, the time domain fit is close in terms of amplitude, yet in the frequency domain there is a mismatch at lower frequencies governed by the source effects at this near-field station. Some local peaks observed in the recorded spectra are also smoothed by the simulated data despite the overall match. This is most probably due to the local site response at this soil station that could not simulated effectively. We note that, similar to results for the Javakheti earthquake simulations, the misfits between the observed and simulated records mostly arise due to the inherent limitations of the stochastic method used but overall the matches are acceptable. Similarly, Figs. 20 and 21, respectively, represent the misfit functions for IRI and ONB stations for the simulations of the 29 April 1991 Racha earthquake.

Table 3

Information on Strong Motion Stations
which recorded the 29 April 1991 Racha earthquake

Station code and name	Latitude (N)	Longitude (E)	Site class	Epicentral distance [km]
BGD Gogdanovka	41.265	43.600	soil	135
IRI	42.517	43.551	soil	25
ONB Oni base camp	42.573	43.436	soil	15

For further validation of the input parameters, we also simulated the 3 May 1991 Racha ($Mw = 5.6$) and 7 April ($Mw = 5.4$) earthquakes which yielded similar results in terms of fits and misfits between the records and simulations. However, for space reasons, we omit those results herein.

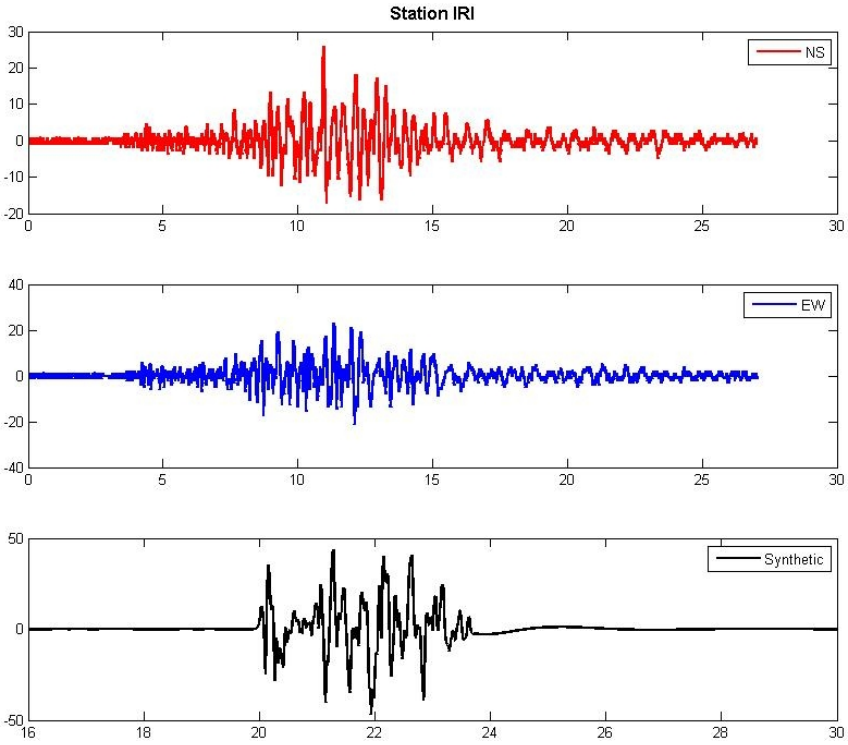

Fig. 16. Simulation results for Racha earthquake (29 April 1991) at IRI station. The observed *versus* simulated acceleration time histories.

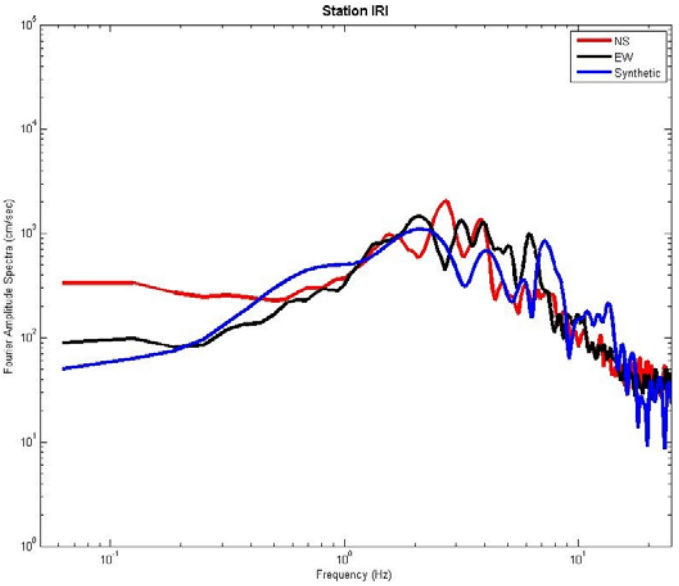

Fig. 17. Simulation results for Racha earthquake (29 April 1991) at IRI station. Fourier amplitude spectra.

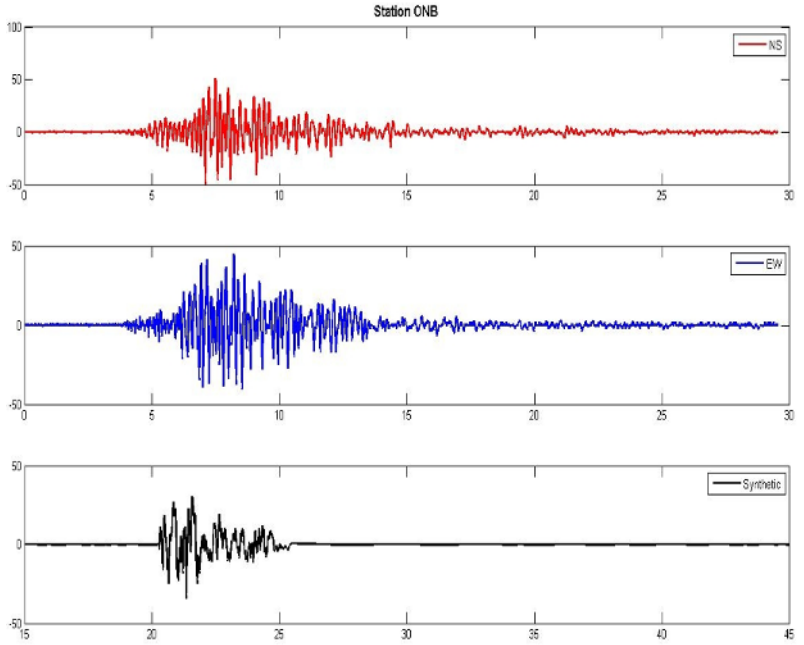

Fig. 18. Simulation results for Racha earthquake (29 April 1991) at ONB station. The observed *versus* simulated acceleration time histories.

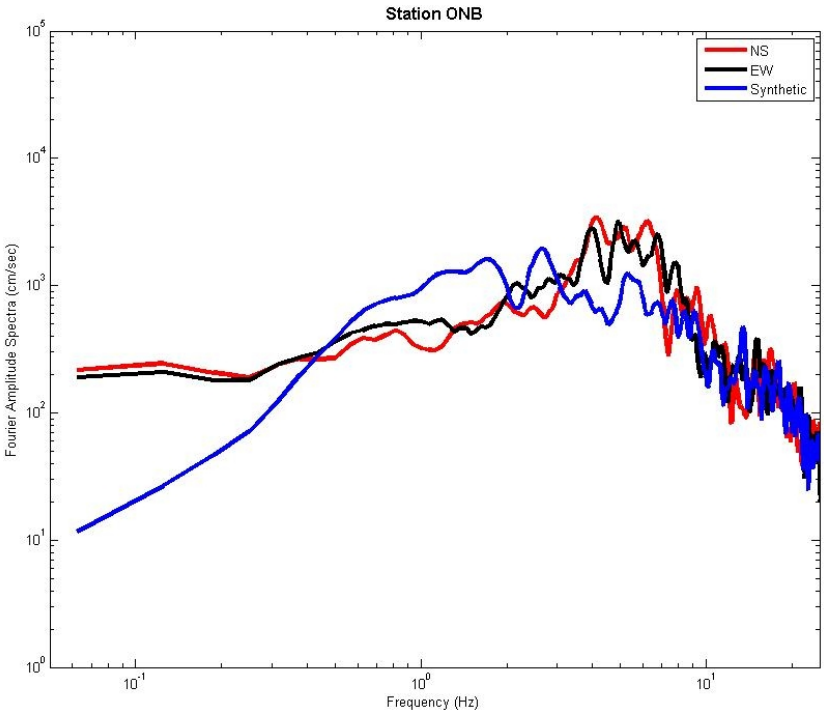

Fig. 19. Simulation results for Racha earthquake (29 April 1991) at ONB station. Fourier amplitude spectra.

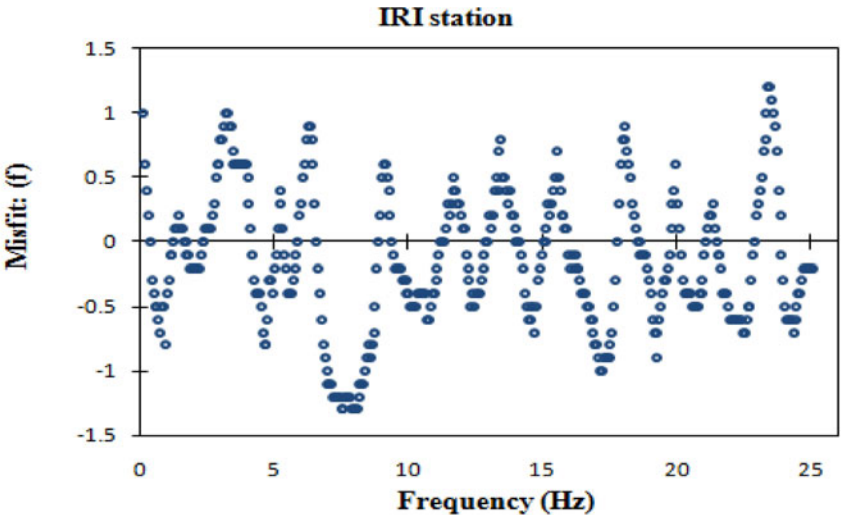

Fig. 20. Misfit function for the 29 April 1991 Javakheti earthquake simulation at IRI station.

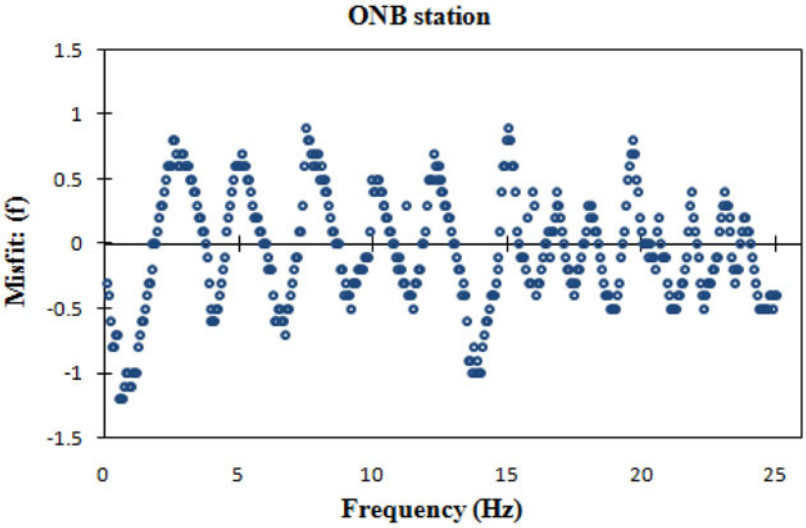

Fig. 21. Misfit function for the 29 April 1991 Javakheti earthquake simulation at ONB station.

5.4 Hybrid-empirical ground motion analyses for Georgia

After the verification of the simulation input parameters of Georgia through the mainshock simulations presented in the previous section, we performed ground motion simulations for a set of scenario events in both host and target regions. Target regions are Javakheti and Racha areas in Georgia while as the host regions with the strike-slip tectonics, eastern end of the North Anatolian Fault zone (Erzincan region) are selected. As the host area with the reverse mechanism, Tabas region in Iran is employed. We note that we originally worked on both the western and eastern parts of NAFZ but finally employed the simulations on the eastern segments since the eastern sections are closer to Georgia in terms of both physical distance and tectonic structure.

The scenario set of simulations to be used in the hybrid-empirical ground motion analyses are performed for Mw = 4-7.5 where $\Delta Mw = 0.25$. The distance range of the dummy stations in the simulations is taken to be $R_{jb} \leq$ 100 km where the locations of the stations are sampled randomly. We note that the simulations are performed for rock conditions in both host and target regions in order to avoid the local site effects which might not be accurately obtained or incorporated. Table 4 displays the seismological parameters used in scenario events for Iran and Turkey which are adopted from Ma'hood *et al.* (2009), Ugurhan and Askan (2010), and Askan *et al.* (2013). We note that the seismological parameters in host regions adopted from these references

Table 4

Seismological parameters used for the scenario simulations in host regions

Parameter	Tabas (Iran)	NAFZ (Turkey)
Magnitude-fault size relationship	Wells and Coppersmith (1994)	Wells and Coppersmith (1994)
Stress drop-fault size relationship	Mohammadioun and Serva (2001)	Mohammadioun and Serva (2001)
Geometric spreading model		
1st hinge in geometric atten.	30.0	30.0
2nd hinge in geometric atten.	100.0	100.0
1st slope in geometric atten.	–1.0	–1.0
2nd slope in geometric atten.	–0.6	–0.5
3rd slope in geometric atten.	–0.5	–0.5
$Q = Q_0 f''(Q_0, n)$	(53, 1.02)	(122, 0.68)
Duration model	$T_R + 0.05\,R$	$T_R + 0.05\,R$
Kappa	0.04	0.035
Beta (Vs) [km/s]	3.2	3.7
Density [g/cm^3]	2.7	2.8
Rupture vel. / S-wave vel.	0.8	0.8
Window applied	Saragoni-Hart	Saragoni-Hart
Site amplifications	Generic rock conditions	Generic rock conditions

were validated robustly against observations in simulations of several past earthquakes. Thus, validations of parameters for previous events will not be repeated herein. Next, the seismological parameters used in scenario events for the target regions (Javakheti and Racha) are presented in Table 5.

We note that the finite-fault source parameters for the scenario simulations are determined based on empirical relationships based on worldwide data (Wells and Coppersmith 1994, Mohammadioun and Serva 2001) which express the fault dimensions and stress drop values in terms of magnitude for different faulting types. Another source term affecting particularly the near-field ground motions is the slip distribution on the fault plane. In this study, for both host and target regions, we employed randomly assigned slip weights to the scenario events with different magnitudes in order to add more inherent variability to the results.

For space reasons, we present herein only a selected set of seismological-based adjustment factors in Figs. 22-23 for PGA and SA ($T = 1$ s) for Turkey–Georgia and Iran–Georgia applications for selected magnitude levels. It is observed from Fig. 22 that for smaller magnitude levels ($Mw = 4.0$ and

Table 5

Seismological parameters used for the scenario simulations in target regions

Parameter	Racha	Javakheti
Magnitude-fault size relationship	Wells and Coppersmith (1994)	Wells and Coppersmith (1994)
Stress drop-fault size relationship	Mohammadioun and Serva (2001)	Mohammadioun and Serva (2001)
Geometric spreading model		
1st hinge in geometric atten.	30.0	30.0
2nd hinge in geometric atten.	100.0	100.0
1st slope in geometric atten.	–1.0	–1.0
2nd slope in geometric atten.	–1	–1
3rd slope in geometric atten.	–1	–1
$Q = Q_0 f^n (Q_0, n)$	(77, 0.937)	(37, 1.089)
Duration model	$T_R + 0.05\ R$	$T_R + 0.05\ R$
Kappa	0.045	0.051
Beta (*Vs*) [km/s]	3.2	3.7
Density [g/cm^3]	2.7	2.8
Rupture vel. / *S*-wave vel.	0.8	0.8
Window applied	Saragoni-Hart	Saragoni-Hart
Site amplifications	Generic rock conditions	Generic rock conditions

5.0) the adjustment factors for PGA are mostly greater than unity for near-field distances and they decrease with distance. The distance variation of the adjustment factors resembles the attenuation of recorded ground motion data. This is not surprising as the adjustment factors are ratios of modeled ground motions in the target region to those in the host region. For larger magnitudes, the adjustment factors take smaller values and they tend to scatter rather than a decreasing trend with distance. This observation is expected as the finite-fault source effects start to govern the amplitudes for the larger events while path attenuation and geometrical spreading factors are more predominant for smaller magnitude levels. Particularly, the effect of random slip weights and finite fault effects arising from azimuthal differences of dummy stations with similar source-to-site distances with respect to the large fault planes is believed to cause the scatter in adjustment factors for $Mw = 6.0$ and 7.0 cases. Figure 23 leads to similar conclusions with lower values of the adjustment factors for SA (1 s) than those for PGA. This finding is consistent with results of Campbell (2003) where consistently smaller adjustment factors are obtained for spectral accelerations at increasing peri-

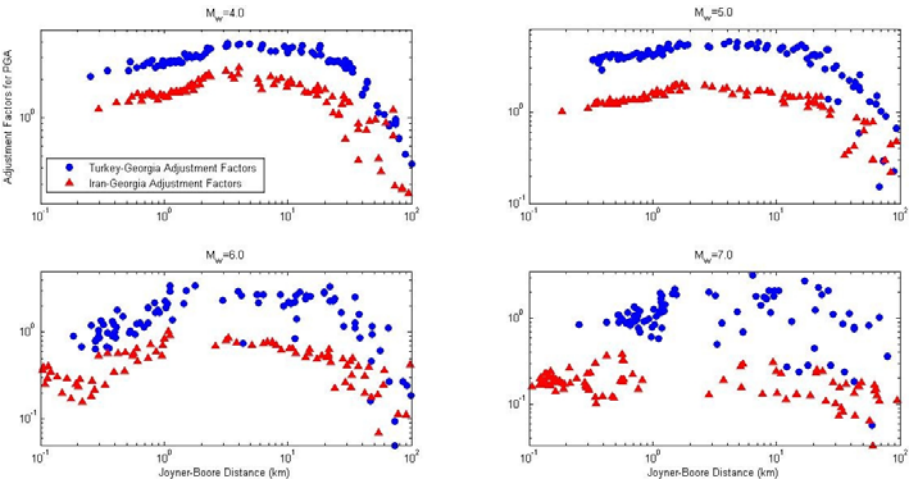

Fig. 22. Seismological-based adjustment factors between the host and target regions for PGA.

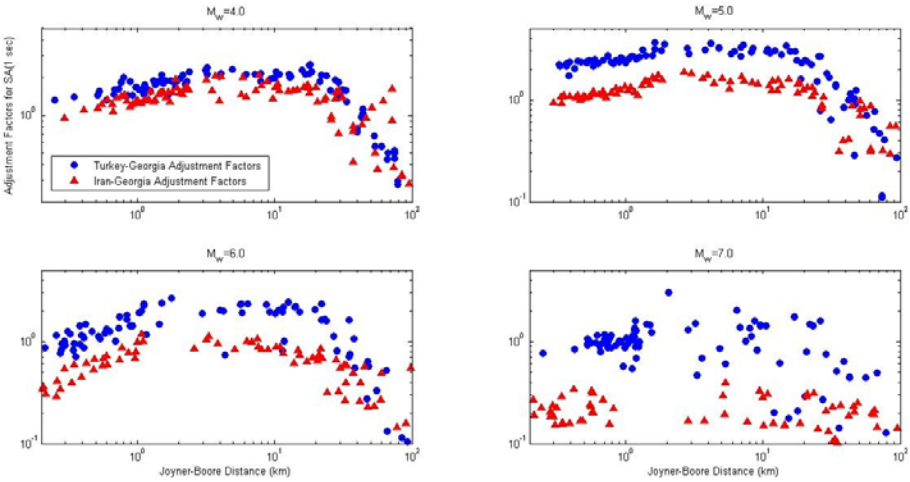

Fig. 23. Seismological-based adjustment factors between the host and target regions for SA (1 s).

ods in comparison to those for PGA. Finally, when the adjustment factors for Turkey–Georgia and Iran–Georgia applications are compared among themselves, for both PGA and SA (1 s), it is seen that the adjustment factors of Iran–Georgia application take smaller values (mostly around unity), particularly for smaller magnitudes, indicating a similarity between the seismological parameters in these regions. Similarly, one can conclude that the modeled ground motions in Turkey and Georgia have larger differences among them-

selves causing larger adjustment factors regardless of the magnitude levels. In summary, the differences in Figs. 22 and 23 are attributed to the variations in the modeled ground motions reflecting the regional characters of the host and target areas as well as the random scatter due to the stochastic method employed herein.

Next, we present comparisons of the hybrid-empirical estimates for a selected event with the real records of the corresponding earthquake. We select 15 June 1991 ($Mw = 6.1$) Georgia event which was not used in the verification simulations to compare with the hybrid-empirical estimates. The original hybrid-empirical method (Campbell 2003) suggests the use of empirical models that work effectively with the data in host regions. Herein, the empirical estimate of ground motion in host region is obtained using Boore and Atkinson (2008) and Akkar *et al.* (2010) models with equal weights of 0.5. The latter GMPE is formed with ground motion data from events that occurred in Turkey while Boore and Atkinson (2008) incorporated worldwide datasets including those from Turkey. They are both shown previously to represent the attenuation of real and simulated ground motions from earthquakes that occurred in Turkey (Ugurhan and Askan 2010, Askan *et al.* 2013).

We observe in Figs. 24-25 that the hybrid-empirical model estimates match the limited number of observations closely. There is some scatter in the hybrid-empirical estimates due to the scatter in the seismological-based adjustment factors arising from several factors including finite fault effects and randomness involved with the stochastic method. Finally, combining two GMPEs to form the hybrid-empirical estimates also contributes to the scatter. Herein, in order to show the original variation in the first hybrid-empirical estimates for Georgia, we do not perform any sampling or averaging. Still, the fit with the limited amount of observed data is promising.

Since the previously-proposed empirical GMPEs for Georgia employ different distance-metrics than our hybrid-empirical estimates, we cannot compare them with our results directly herein without introducing distance-conversion errors. Yet, to see indirectly the differences between the previous empirical models and our hybrid-empirical ground motion estimates, we plot the GMPEs by Smit *et al.* (2000) and Slejko *et al*. (2008) against the data from 15 June 1991 ($Mw = 6.1$) Georgia event in Fig. 26. Despite the limited data, in comparison with Fig. 24, it is observed that the hybrid-empirical estimates proposed in this study provide a closer match with the attenuation of the data.

Finally, we note that we presented the median hybrid empirical ground motion estimates in Figs. 24-25. The standard deviations of hybrid-empirical models involve the aleatory uncertainties of the GMPEs used for the host region as well as the epistemic uncertainty of the simulations. In this study, a

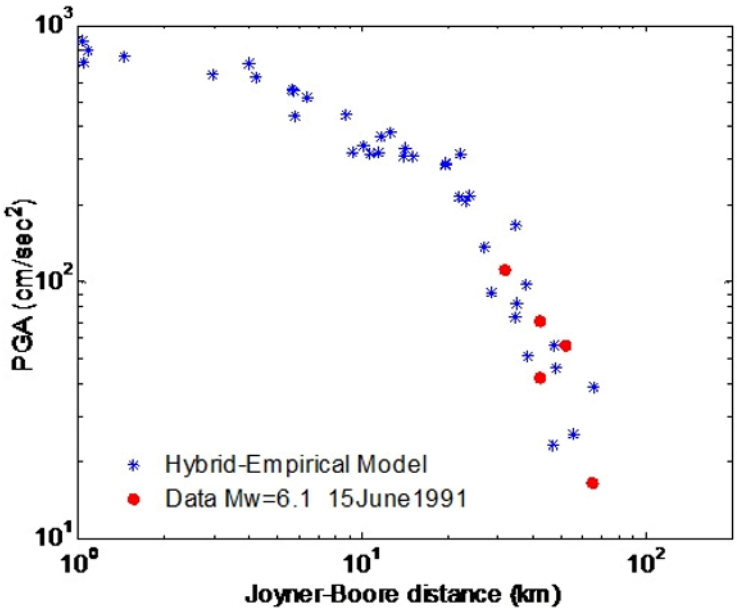

Fig. 24. Comparison of the hybrid-empirical estimates for PGA against data of the 15 June 1991 earthquake (Mw = 6.1).

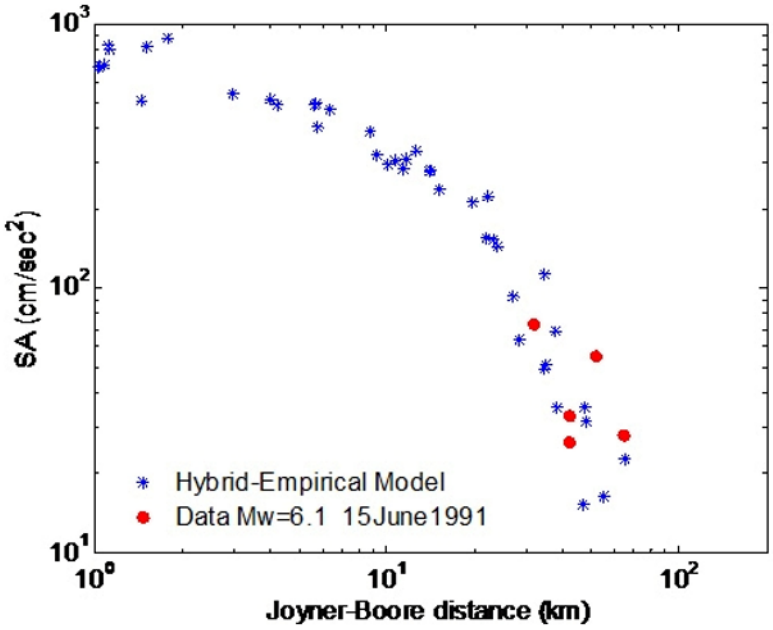

Fig. 25. Comparison of the hybrid-empirical estimates for SA at 1 s against data of the 15 June 1991 earthquake (Mw = 6.1).

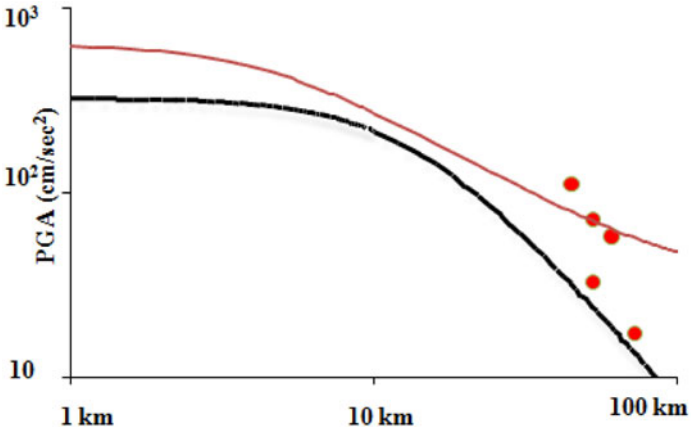

Fig. 26. Comparison of the previous empirical GMPEs proposed for Georgia in terms of PGA against data of the 15 June 1991 earthquake ($Mw = 6.1$). Red curve is the GMPE by Smit *et al.* (2000), the black curve is the GMPE by Slejko *et al.* (2008), and the red dots are the observed data of the 15 June 1991 earthquake.

quantification of the parameter uncertainties is not performed since the target simulations are performed with only a single value for each seismic input parameter. The proposed set of ground motion estimations is an initial step for a hybrid-empirical model for Georgia. As the studies related to derivation of model parameters in the region progress, it is always possible to quantify the errors from using alternative parameters in the simulations.

6. SUMMARY AND CONCLUSIONS

Georgia, despite being located in a seismically active region, does not have sufficiently strong ground motion data to build empirical ground motion models. Existing previous ground motion models are commonly used; however, they need to be augmented for robust applications in earthquake engineering and seismology. In this study, we have applied the hybrid-empirical method to two regions in Georgia with different source mechanisms: Javakheti and Racha regions. According to the tectonic regime of the target areas, two regions have been chosen as a host region. One of them is the North Anatolian Fault zone in Turkey with mostly strike-slip stress regime and the other is Tabas in Iran with mostly reverse mechanism. We performed stochastic finite-fault simulations in both host and target areas and employed the hybrid-empirical method of Campbell (2003). As a result, we developed an initial set of hybrid empirical ground motion estimations for PGA and SA at selected periods for Georgia. Comparison of the proposed model for a specific case (15 June 1991, $Mw = 6.1$ event in Georgia) with the corre-

sponding observed data reveals a close match with the limited amount of available data.

In this study, we have not performed regression analyses to the hybrid-empirical ground motion estimates; however, it is possible to form hybrid-empirical models for Georgia. Indeed, derivation of ground motion models based on these coefficients for use in regional PSHA in Georgia is now in progress. Potential future research includes the test and use of such hybrid-empirical models for a variety of engineering seismology and earthquake engineering purposes.

Acknowledgments. This study is supported by the Earthquake Model of the Middle East (EMME) project. Authors would like to thank Beliz Ugurhan and Irina Khvedelidze for their help in some of the calculations.

References

Akkar, S., and J. Bommer (2006), Influence of long-period filter cut-off on elastic spectral displacements, *Earthq. Eng. Struct. Dyn.* **35**, 9, 1145-1165, DOI: 10.1002/eqe.577.

Akkar, S., Z. Cagnan, E. Yenier, E. Erdogan, M.A. Sandikkaya, and P. Gulkan (2010), The recently compiled Turkish strong-motion database: preliminary investigation for seismological parameters, *J. Seismol.* **14**, 3, 457-479, DOI: 10.1007/s10950-009-9176-9.

Akkar, S., O. Kale, E. Yenier, and J.J. Bommer (2011), The high-frequency limit of usable response spectral ordinates from filtered analogue and digital strong-motion accelerograms, *Earthq. Eng. Struct. Dyn*. **40**, 12, 1387-1401, DOI: 10.1002/eqe.1095.

Allen, M., J. Jackson, and R. Walker (2004), Late Cenozoic reorganization of the Arabia-Eurasia collision and the comparison of short-term and long-term deformation rates, *Tectonics* **23**, 2, TC2008, DOI: 10.1029/2003TC001530.

Ambraseys, N., P. Smit, R. Berardi, D. Rinaldis, F. Cotton, and C. Berge-Thierry (2000), European strong-motion database, European Council, Environment and Climate Research Programme, Imp. College – ENEA – IPSN – Servizio Sismico – Sogin (CD rom).

Ambraseys, N., J. Douglas, R. Sigbjornsson, C. Berge-Thierry, P. Suhadolc, G. Costa, and P. Smit (2004), European strong-motion database, Vol. 2, Imp. College – Earthq. Eng. Res. Center – IRSN – Univ. Trieste (CD rom).

Amiri, G.G., A. Mahdavian, and F.M. Dana (2007), Attenuation relationships for Iran, *J. Earthq. Eng*. **11**, 4, 469-492, DOI: 10.1080/13632460601034049.

Askan, A., F.N. Sisman, and B. Ugurhan (2013), Stochastic strong ground motion simulations in sparsely-monitored regions: A validation and sensitivity

study on the 13 March 1992 Erzincan (Turkey) earthquake, *Soil Dyn. Earthq. Eng.* **55**, 170-181, DOI: 10.1016/j.soildyn.2013.09.014.

Bommer, J.J., and N.A. Abrahamson (2007), Reply to "Comment on «Why do modem probabilistic seismic-hazard analyses often lead to increased hazard estimates?» by Julian J. Bommer and Norman A. Abrahamson" by Jens-Uwe Klugel, *Bull. Seismol. Soc. Am.* **97**, 6, 2215-2217, DOI: 10.1785/0120070099.

Bommer, J.J., J. Douglas, and F.O. Strasser (2003), Style-of-faulting in ground motion prediction equations, *Bull. Earthq. Eng.* **1**, 2, 171-203, DOI: 10.1023/A:1026323123154.

Boore, D.M. (2004), Can site response be predicted? *J. Earthq. Eng.* **8**, 1, 1-41, DOI: 10.1142/S1363246904001651.

Boore, D.M., and G.M. Atkinson (2008), Ground-motion prediction equations for the average horizontal component of PGA, PGV, and 5%-damped PSA at spectral periods between 0.01 s and 10.0 s, *Earthq. Spectra* **24**, 1, 99-138, DOI: 10.1193/1.2830434.

Cagnan, Z. (2013), Ground motion prediction models for crustal and deep earthquakes in eastern Mediterranean Region based on host-to-target method. **In:** *Proc. 2nd Turkish Earthquake Engineering and Seismology Conference, 25-27 September 2013, Hatay, Turkey* (in Turkish).

Campbell, K.W. (2003), Prediction of strong ground motion using the hybrid empirical method and its use in the development of ground-motion (attenuation) relations in eastern North America, *Bull. Seismol. Soc. Am.* **93**, 3, 1012-1033, DOI: 10.1785/0120020002.

Cotton, F., F. Scherbaum, J.J. Bommer, and H. Bungum (2006), Criteria for selecting and adjusting ground-motion models for specific target applications: Applications to Central Europe and rock sites, *J. Seismol*. **10**, 2, 137-156, DOI: 10.1007/s10950-005-9006-7.

DeMets, C., R. Gordon, D. Argus, and S. Stein (1990), Current plate motions, *Geophys. J. Int*. **101**, 2, 425-478, DOI: 10.1111/j.1365-246X.1990.tb06579.x.

Douglas, J. (2003), Earthquake ground motion estimation using strong-motion records: a review of equations for the estimation of peak ground acceleration and response spectral ordinates, *Earth-Sci. Rev.* **61**, 1-2, 43-104, DOI: 10.1016/S0012-8252(02)00112-5.

Douglas, J., H. Bungum, and F. Scherbaum (2005), Ground-motion prediction equations for southern Spain and southern Norway obtained using the composite model perspective, *J. Earthq. Eng.* **10**, 1, 33-72, DOI: 10.1142/S1363246906002566.

Jackson, J., and N. Ambraseys (1997), Convergence between Eurasia and Arabia in eastern Turkey and the Caucasus. **In:** D. Giardini and S. Balassanian (eds.), *Historical and Prehistorical Earthquakes in the Caucasus*, Kluwer Academic Publishers, Dordrecht, 79-90.

Ma'hood, M., H. Hamzehloo, and G.J. Doloei (2009), Attenuation of high frequency *P* and *S* waves in the crust of the East-Central Iran, *Geophys. J. Int.* **179**, 3, 1669-1678, DOI: 10.1111/j.1365-246X.2009.04363.x.

Mohammadioun, B, and L. Serva (2001), Stress drop, slip type, earthquake magnitude, and seismic hazard, *Bull. Seismol. Soc. Am*. **91**, 4, 694-707, DOI: 10.1785/0120000067.

Motazedian, D., and G.M. Atkinson (2005), Stochastic finite-fault modeling based on a dynamic Corner frequency, *Bull. Seismol. Soc. Am.* **95**, 3, 995-1010, DOI: 10.1785/0120030207.

Pezeshk, S., A. Zandieh, and B. Tavakoli (2011), Hybrid empirical ground-motion prediction equations for eastern North America using NGA models and updated seismological parameters, *Bull. Seismol. Soc. Am*. **101**, 4, 1859-1870, DOI: 10.1785/0120100144.

Rautian, T.G. (1960), Earthquake energy transactions, *Joint Inst. Phys. Earth. Acad. Sci. USSR* **9**, 35-114.

Reilinger, R., S. McClusky, Ph. Vernant, S. Lawrence, S. Ergintav, R. Cakmak, H. Ozener, F. Kadirov, I. Guliev, R. Stepanyan, M. Nadariya, G. Hahubia, S. Mahmoud, K. Sakr, A. Ar-Rajehi, D. Paradissis, A. Al-Aydrus, M. Prilepin, T. Guseva, E. Evren, A. Dmitrotsa, S.V. Filikov, F. Gomez, R. Al-Ghazzi, and G. Karam (2006), GPS constraints on continental deformation in the Africa–Arabia–Eurasia continental collision zone and implications for the dynamics of plate interactions, *J. Geophys. Res*. **111**, B5, B05411, DOI: 10.1029/2005JB004051.

Riznichenko, Iu.V. (1992), *Problems of Seismology: Selected Papers*, Springer, 445 pp.

Shengelia, I., Z. Javakhishvili, and N. Jorjiashvili (2011), Coda wave attenuation for three regions of Georgia (Sakartvelo) using local earthquakes, *Bull. Seismol. Soc. Am.* **101**, 5, 2220-2230, DOI: 10.1785/0120100326.

Shoja-Taheri, J., and H. Ghofrani (2007), Stochastic finite-fault modeling of strong ground motions from the 26 December 2003 Bam, Iran, earthquake, *Bull. Seismol. Soc. Am*. **97**, 6, 1950-1959, DOI: 10.1785/0120060059.

Slejko, D., Z. Javakhishvili, A. Rebez, M. Santulin, M. Elashvili, P.L. Bragato, T. Godoladze, and J. Garcia (2008), Seismic hazard assessment for the Tbilisi test area (eastern Georgia), *Boll. Geofis. Teor. Appl.* **49**, 1, 37-57.

Smit, P., V. Arzoumanian, Z. Javakhishvili, S. Arefiev, D. Mayer-Rosa, S. Balassanian, and T. Chelidze (2000), The digital accelerograph network in the Caucasus. **In:** S. Balassanian *et al*. (eds.), *Earthquake Hazard and Seismic Risk Reduction*, Advances in Natural and Technological Hazards Research, Vol. 12, 109-118, DOI: 10.1007/978-94-015-9544-5_12.

Sokolov, V. (1997), Empirical models for estimating Fourier-amplitude spectra of ground acceleration in the northern Caucasus (Racha seismogenic zone), *Bull. Seismol. Soc. Am.* **87**, 6, 1401-1412.

Ugurhan, B., and A. Askan (2010), Stochastic strong ground motion simulation of the 12 November 1999 Düzce (Turkey) earthquake using a dynamic Corner frequency approach, *Bull. Seismol. Soc. Am.* **100**, 4, 1498-512, DOI: 10.1785/0120090358.

Varazanashvili, O., N. Tsereteli, and E. Tsereteli (2011), Historical Earthquakes in Georgia (up to 1900): Source Analysis and Catalogue Compilation, Limited "MVP", Tbilisi.

Varazanashvili, O., N. Tsereteli, A. Amiranashvili, E. Tsereteli, E. Elizbarashvili, J. Dolidze, L. Qaldani, M. Saluqvadze, Sh. Adamia, N. Arevadze, and A. Gventcadze (2012), Vulnerability, hazards and multiple risk assessment for Georgia, *Nat. Hazards* **64**, 3, 2021-2056, DOI 10.1007/s11069-012-0374-3.

Wells, D.L., and K.J. Coppersmith (1994), New empirical relationships among magnitude, rupture length, rupture width, rupture area, and surface displacement, *Bull. Seismol. Soc. Am*. **84**, 4, 974-1002.

Zafarani, H., A. Noorzad, A. Ansari, and K. Bargi (2009), Stochastic modeling of Iranian earthquakes and estimation of ground motion for future earthquakes in Greater Tehran, *Soil Dyn. Earthq. Eng.* **29**, 4, 722-741, DOI: 10.1016/j.soildyn.2008.08.002.

Zare, M., H. Amini, P. Yazdi, K. Sesetyan, M.B. Demircioglu, D. Kalafat, M. Erdik, D. Giardini, M. Asif Khan, and N. Tsereteli (2014), Recent developments of the Middle East catalog, *J. Seismol.* **18**, 4, 749-772, DOI: 10.1007/s10950-014-9444-1.

Received 24 November 2014
Received in revised form 19 August 2015
Accepted 17 September 2015